Published in final edited form as:
Nat Mater. 2012 December ; 11(12): 1065–1073. doi:10.1038/nmat3468.

Ultrasmall implantable composite microelectrodes with bioactive surfaces for chronic neural interfaces

Takashi D. Yoshida Kozai[1,*], **Nicholas B. Langhals**[1], **Paras R. Patel**[1], **Xiaopei Deng**[2], **Huanan Zhang**[2], **Karen L. Smith**[3], **Joerg Lahann**[2], **Nicholas A. Kotov**[2,*], and **Daryl R. Kipke**[1,*]

[1]Neural Engineering Lab, Department of Biomedical Engineering, College of Engineering, University of Michigan, Ann Arbor, Michigan 48109, USA

[2]Department of Chemical Engineering, College of Engineering, University of Michigan, Ann Arbor, Michigan 48109, USA

[3]Center for Neural Communication Technology, New York State Department of Health, Wadsworth Center, Albany, New York 12201, USA.

Abstract

Implantable neural microelectrodes that can record extracellular biopotentials from small, targeted groups of neurons are critical for neuroscience research and emerging clinical applications including brain-controlled prosthetic devices. The crucial material-dependent problem is developing microelectrodes that record neural activity from the same neurons for years with high fidelity and reliability. Here, we report the development of an integrated composite electrode consisting of a carbon-fibre core, a poly(*p*-xylylene)-based thin-film coating that acts as a dielectric barrier and that is functionalized to control intrinsic biological processes, and a poly(thiophene)-based recording pad. The resulting implants are an order of magnitude smaller than traditional recording electrodes, and more mechanically compliant with brain tissue. They were found to elicit much reduced chronic reactive tissue responses and enabled single-neuron recording in acute and early chronic experiments in rats. This technology, taking advantage of new composites, makes possible highly selective and stealthy neural interface devices towards realizing long-lasting implants.

[*]tkozai@umich.edu; kotov@umich.edu; dkipke@umich.edu..

Author contributions

T.D.Y.K., N.B.L., J.L., N.A.K. and D.R.K. planned the project. Carbon fibres were provided by H.Z. MTEs were assembled by T.D.Y.K. and P.R.P. CVD parameters were designed by X.D., and CVD was carried out by X.D. and T.D.Y.K. PEGMA coatings and biofouling testing were carried out by X.D. Raman spectroscopy data were analysed by X.D. PEDOT deposition parameters were designed by N.B.L. and T.D.Y.K. and carried out by P.R.P. and T.D.Y.K. P.R.P. and T.D.Y.K. also conducted *in vitro* characterization of the devices. SEM imaging and energy-dispersive X-ray analysis was carried out by H.Z. *In vivo* recordings were carried out by N.B.L. and T.D.Y.K. Chronic *in vivo* experiments were planned, carried out and analysed by T.D.Y.K. Data analysis was carried out by N.B.L. and T.D.Y.K. K.L.S. led and carried out the two-photon immunohistochemistry and imaging for the chronic implant. Cryo-immunohistochemistry was planned by P.R.P. and T.D.Y.K. and conducted by T.D.Y.K. T.D.Y.K. and D.R.K. wrote the manuscript. All authors discussed the results.

Additional information

Supplementary information is available in the online version of the paper. Reprints and permissions information is available online at www.nature.com/reprints. Correspondence and requests for materials should be addressed to T.D.Y.K., N.A.K. and D.R.K.

Competing financial interests

D.R. Kipke has a significant financial and leadership interest in NeuroNexus Technologies, a company specializing in neural interface devices. At the time of this study, N.B. Langhals was a consultant for NeuroNexus Technologies.

Obtaining selective, high-fidelity, long-lasting readouts of brain activity is a critical technology across basic and applied neuroscience. Since the pioneering work of Strumwasser, demonstrating the ability to chronically record neural activity using microwires in hibernating squirrels[1], there has been an ongoing push to improve implantable microelectrode technologies in terms of size, shape, density, recording mode, signal-to-noise ratio (SNR), tissue integration and functional duration[2,3]. Today, most implantable neural microelectrodes trace back to the three historical microelectrode technologies: microwires; thin-film planar probes based on silicon or polymer substrates; or bulk micromachined arrays. Although incremental progress has been steady, there are still no definitive solutions for creating stable, long-lasting devices that elicit little or no deleterious tissue responses in the brain[2,4]. As recent advances in the understanding of brain tissue responses come to the forefront of neural engineering[5–9], advances of these technologies are reaching limitations imposed by size, flexibility, strength, biocompatibility and electrical trade-offs of traditional materials such as metals, glass and silicon. To make fundamental advances in microelectrode technologies, it is necessary to bring together a new set of materials to create functional chronic implantable electrodes that are much smaller and more flexible, but sufficiently robust, and at the same time have improved electrical characteristics and bioactive surfaces to control intrinsic biological processes.

Emerging trends and technology in advanced biomaterials[10] and chronic neural interfaces[5,11,12] involve bio-inspired exploration of new paradigms to improve the biocompatibility and lifetime, better tissue integration and maintain neuronal viability. Although carbon-fibre microelectrodes have been extensively used to record extracellular/intracellular neural activity and changes in chemical concentrations, they are insulated in glass capillaries or fused-silica tubes, which increase the implanted device's footprint and stiffness[13–15] and limit its capabilities for chronic *in vivo* single-unit recordings. Studies of the probe/tissue interface suggest that flexible probes may help to minimize perpetual mechanical trauma caused by physiological motion between the probe and the surrounding tissue[9,16–20]. To this end, polymers have been employed in increasingly flexible probes[21–23]. Furthermore, new fabrication techniques leveraging softer advanced materials have allowed for sophisticated types of probe architecture with subcellular-sized features demonstrating a reduction of the encapsulation response[24]. However, reduction of recording sites causes an inverse effect of increasing impedance despite its ideal characteristics for isolating single-unit neural activity. Therefore, advanced organic conductive polymers such as poly(3,4-ethylenedioxythiophene) (PEDOT) have been used to improve the recording characteristics of small recording sites over time[10], although PEDOT has been shown to cause some degradation from prolonged electrical stimulation[25]. More recently, functional organic bioactive surface materials have shown promise of improving chronic interfaces in new ways[26]. The emerging engineering model based on these studies points to innovative composite materials that are specifically designed to fulfill aggressive sets of functional requirements across multiple dimensions that were previously limited by intrinsic size, strength, flexibility, electrical and biocompatibility trade-offs.

Our objective was to fabricate and test an ultrasmall organic electrical microelectrode that has a subcellular cross-sectional dimension, but is flexible, stronger, and has sufficient electrical characteristics for neural recording and advanced bioactive capabilities for controlling intrinsic biological processes. We developed composite materials that are specifically engineered to extend the microelectrode design space to achieve a set of functional requirements for chronic performance that previously were limited by intrinsic size, strength and electrical trade-offs of conventional technologies. The resulting microthread electrodes (MTEs) were prepared by mounting 7-μm-diameter carbon fibres onto a microelectrode printed circuit board. The carbon fibre was then coated with an 800 nm poly(*p*-xylylene) coating using chemical vapour deposition (CVD) polymerization (Fig.

1a and Supplementary Figures). Poly(*p*-xylylene) (also known as parylene-N) was selected for its very low dissipation factor, high dielectric strength and low dielectric constant that is also invariant with frequency. A 50-nm-thick layer of the functionalized polymer poly((*p*-xylylene-4-methyl-2-bromoisobutyrate)-*co*-(*p*-xylylene)) was deposited onto the poly(*p*-xylylene)-coated fibre using CVD polymerization[27] (Fig. 1b). This polymer provides initiator groups for subsequent atom transfer radical polymerization[28] (ATRP). By ATRP, a ~200-nm-thick poly(ethylene glycol) methacrylate (PEGMA) top layer was deposited, which rendered the neuronal probe devices protein-resistant[28,29] (Fig. 1c). Finally, a recording site was created by electrochemical deposition of poly(3,4-ethylenedioxythiophene)/poly(styrenesulphonate) (PEDOT:PSS) onto the tip of the neuronal probe, from which the poly(*p*-xylylene) and PEGMA coatings had previously been removed (Fig. 1d). The primary innovation of this technology is the combination of advanced materials to create an ultrasmall organic interface that has the approximate size of a single trace on a conventional silicon neural probe, but sufficient strength and flexibility to act as a stand-alone electrode.

The MTE electrical properties were characterized by electrochemical impedance spectroscopy (EIS) and cyclic voltammetry. Measurements were taken for two controls: poly(*p*-xylylene)-insulated carbon fibres, and poly(*p*-xylylene)-insulated fibres with a ~38.5 μm^2 exposed cut carbon tip. Last, poly(*p*-xylylene)-insulated MTEs with recording sites and increasing degrees of PEDOT:PSS deposition were characterized. EIS measurements showed a progressive decrease in impedance as the insulation at the tip was removed, as well as with increasing PEDOT deposition (Fig. 2a). The phase diagram also shows decreasing phase delay with increasing PEDOT deposition, which is a hallmark of PEDOT-coated electrical sites[30] (Fig. 2b). Cyclic voltammetry measurements also showed increased charge storage capacity with increasing PEDOT deposition (Fig. 2c), which could be relevant for brain stimulation devices. Cyclic voltammetry profiles indicate the presence of PEDOT on the recording site.

The MTEs also have an essential combination of mechanical properties for neural probes in terms of stiffness, strength and size (Supplementary Fig. S3). The stiffness (k) of a MTE calculated from the cross-sectional area (A), elastic modulus (E) and length implanted into the cortex (l) is 4,540 N m^{-1}, which is an order of magnitude smaller than for a conventional silicon microelectrode of the same length, ~151,000 N m^{-1} (ref. 18). The cantilever beam spring constant (k_c) for a conventional silicon microelectrode is 2.13 N m^{-1} in the direction normal to the recording surface and 143 N m^{-1} in the lateral direction, whereas k_c for the MTE is 0.0106 N m^{-1} in all radial directions. This reduced stiffness or improved compliance ($1/k$) is primarily the result of the small-diameter carbon fibre, comparable to the size of cells, and the use of the thin parylene-N coating (Fig. 3a). The k_c is superior over recently developed tunicate-derived nanocomposite probes[31]. Stiff implanted probes tethered to the skull may also cause rupture of the nearby blood brain barrier (BBB) during micromotion or physiological motion[9,17,32].

To prevent biofouling from BBB disruption, the MTEs have a biofouling-resistant surface through functionalization of the outer poly(*p*-xylylene) insulation with PEGMA, an anti-biofouling molecule. Although stab wound studies show limited chronic tissue damage[5], plasma protein adsorption onto the electrode may perpetuate the tissue response in chronically implanted neural electrodes. For example, the plasma protein albumin is, in part, responsible for inducing glial cell activation and proliferation[33,34]. Adsorption of plasma proteins to probe surfaces may perpetuate the release of pro-inflammatory cytokines and their continual adsorption onto the probe surface. Within the central nervous system, anti-biofouling coatings may have to be stable only long enough for cells to repair the BBB and clean up the plasma exudates, thereby allowing attenuation of pro-inflammatory cytokines in

the probe's microenvironment[9]. As such, covalently grafted functional bioactive surface materials may be more effective for improving chronic neural interfaces than rapidly dissolving anti-biofouling hydrogels. Furthermore, although bioactive peptide coatings may denature, their effects have been shown to last for months[26]. The organic PEGMA surface material demonstrated improved anti-biofouling properties from FITC–albumin adsorption compared with the native poly(*p*-xylylene) surface *in vitro* (Fig. 3a–e). The covalently grafted PEGMA layer has the added benefit of further minimizing the microelectrode footprint compared with traditional drug-eluting hydrogels that acutely push tissue away from the electrode surface. To the authors' knowledge, this is the first demonstration of a functionalized poly(*p*-xylylene) coating in a functional neural microelectrode. These properties are especially important when chronic use of the probes is intended.

One important aspect of the unique integration of new functional materials is that it enables a significant reduction in footprint that minimizes insertion damage, while maintaining comparable performance. During insertion, the highly regulated BBB is compromised as the implantation of microelectrodes punctures and tears neural vasculature[9,32,35], leading to plasma release into the surrounding parenchyma. BBB disruption caused by probe insertion leads to a net increase in extracellular water content[36] and intracranial pressure[37] often associated with tissue damage[38]. This acute trauma leads to the release of erythrocytes, and inflammatory factors from disrupted blood vessels, which facilitate recruitment of activated microglia and astrocytes in a broad region around the inserted probe[4,9,11,33]. Minimizing the device footprint is important for minimizing insertion trauma by reducing infiltration of blood components and pro-inflammatory signalling, especially when not using a positional guide to avoid large vasculature deep in the cortex[35]. It can also minimize disrupting arterioles during insertion. Disrupting arterioles causes loss of perfusion to the tissue below the disrupted region where the recording sites are located, leading to further neuronal damage by means of ischaemia[9,35,39]. Furthermore, the smaller feature size reduces the increase in intracranial pressure caused by tissue displacement from the probe footprint, which can improve recordings in acute experiments. However, the challenge with silicon technology is the difficultly in scaling to a single-trace subcellular size while maintaining structural and electrical integrity when fixed to the skull. The MTEs have a total ~8.5 μm diameter, which allows for a subcellular cross-section. Acute histological analysis shows that bleeding is limited around MTE probes (Fig. 3f–h,l). It also demonstrates that these microelectrodes can be implanted into the cortex. On the other hand, substantial bleeding can be observed around a conventional silicon probe (Fig. 3i–l). The improved subcellular structure enabled by the composite material may enhance the interface across multiple dimensions. Key differences between silicon probes and MTE probes have been highlighted in Table 1 (refs 40,41). To the authors' knowledge, this is the smallest electrical microelectrode to be implanted into the cortex as a stand-alone sensor[42].

Two fibre microthread arrays (MTAs) as well as single MTEs were implanted 1.6 mm deep into rat motor cortex (Fig. 4a). MTAs contained one carbon recording site and one PEDOT recording site. MTEs contained either a carbon recording site or a PEDOT recording site. *In vivo* cortical recordings with PEDOT:PSS-deposited poly(*p*-xylylene)/carbon fibres were able to record neural spikes (Fig. 4b). In all *in vivo* trials, the PEDOT:PSS-coated MTE was acutely able to detect at least one neuronal spike with a SNR greater than 4 s.d. On the other hand, poly(*p*-xylylene)-insulated carbon fibres with a cut carbon exposed recording site were unable to record any single unit with an SNR greater than 4 s.d. (Fig. 4b). Finally, an un-insulated carbon fibre implanted 2 mm into the cortex was able to record local field potentials (LFPs), but was unable to discriminate any single-neuron spikes (data not shown). Figure 4c–e shows sorted single-unit activity: pile plot (Fig. 4c), principle component analysis (Fig. 4d) and the mean waveform (Fig. 4e). On the other hand, simultaneous LFP recordings indicated that both materials are able to detect similar activity; however, the

PEDOT:PSS recording site was able to detect LFPs with a higher amplitude (Fig. 4f). A lack of phase difference in the LFP range between carbon and PEDOT:PSS sites (Fig. 4f) also verified that carbon and PEDOT:PSS recording sites can detect similar LFP activities. This is also demonstrated by the power spectral density plot of the neural recordings showing the intensity of the recordings as a function of frequency (Fig. 4g). The peak observed around 9 Hz is representative of low-frequency synchronous activity in the alpha band. These recordings demonstrate the ability to insert and record high-quality unit activity from viable neurons located close to the MTE. To the authors' knowledge, this is the smallest recording site reported so far, smaller than a cell body, but with excellent electrical characteristics.

Initial chronic neural recording studies suggest that these microelectrodes are stable over five weeks in the brain. MTEs demonstrated a high yield across animals for detecting single-unit activity over time (Fig. 5a), which is comparable or better than the yield of conventional silicon devices[10] or wire microelectrode arrays[43]. The mean SNR of the largest discernible single unit detected by each MTE shows the stability of the chronic single-unit recordings (Fig. 5b and Supplementary Fig. S5). This suggests that the poly(*p*-xylylene) insulation and PEDOT recording sites hold up over time, and that they are biocompatible. During the initial inflammation period, the SNR decreases, and then increases temporarily to a peak around one week before stabilizing. Tissue response to stab wounds subsides by four weeks[5], suggesting stabilization of the tissue after surgery. For this reason, electrophysiological recordings were continued up to five weeks. By the second week, the single units seem to stabilize as indicated by the decreased fluctuation and s.d. This stabilization period is similar to that of previously reported studies[10,43]. Deconstructing the mean SNR of the largest discernible single unit to the units' amplitude and the electrodes' noise floor shows that fluctuations in the SNR in the first two weeks are due to variations largely in signal amplitude, as opposed to changes in noise floor (Fig. 5c). Examining individual electrodes for SNR or signal amplitude fluctuations further demonstrates the large variability observed in the first week after implantation, and stabilization after the second week (Fig. 5d and Supplementary Fig. S5). Figure 5e,f,i–l demonstrates two examples of 5+ week chronic recordings from two different animals. These initial chronic recording studies suggest that these microelectrodes remain intact in the brain over moderate lengths of time, without any electrophysiological evidence of signal degradation. They also have an extremely high yield of unit recordings compared with silicon-on-anything probes[10].

Last, recently there has been an improvement in the understanding of the detailed reactive tissue responses to implantable microelectrodes[12]. Tissue encapsulation of the probe and neuronal death in the vicinity of the recording electrode have been implicated as the largest variables negatively impacting the stability and longevity of long-term neural recordings[5,11]. Chronically implanted tethered MTEs show a qualitatively reduced chronic tissue response. MTEs elicit a lesser glial fibrillary acidic protein (GFAP) response in astrocytes compared with the traditional silicon electrode (Fig. 6a,b). More microglia can also be observed immediately adjacent to the planar silicon electrode compared with the MTE as indicated by Iba-1 and Hoechst labels (Fig. 6a,c). Endothelial barrier antigen (EBA) labels healthy BBB. Blood vessels around the silicon electrode show substantial injury compared with the MTE (Fig. 6a,d). Neuronal densities around the silicon electrode are also diminished whereas several neurons can be observed adjacent to the MTE (Fig. 6e and Supplementary Fig. S6). The MTEs show a much reduced chronic tissue response across several histological outcomes over early chronic timescales. These histological data demonstrate the ability of MTEs to have a markedly improved microenvironment in neural interfaces within the recording volume of the MTE and suggest progress towards a stealthy interface with the brain. Future studies should focus on exploring the effects of MTEs with various probe diameters, bioactive coatings and flexibility compliance levels to identify individual and synergistic contributions.

This study brought together a new set of materials to make fundamental advances in microelectrode technology across the dimensions of size, strength, flexibility, surface biochemistry and electrical properties. The results demonstrated that this innovative composite microelectrode with a reduced footprint was able to chronically record single-unit spikes. To the best of the authors' knowledge this is: the smallest stand-alone implantable neuronal ultramicroelectrode; the first functionalized poly(*p*-xylylene) surface on a neural microelectrode; and the smallest recording electrode site to deposit PEDOT:PSS and successfully record chronic single-unit activity in the cortex. Furthermore, emerging PEDOT blends (PEDOT/carbon nanotubes) show promising results of being more stable than PEDOT:PSS (ref. 44). Although these electrodes successfully recorded high-quality neural activity over several weeks, four of the seven implants had a headcap failure around the sixth week associated with poor printed circuit board design, compounded by the animal regularly bumping it into the cage. However, previous studies suggest that recordings become stable around 5–6 weeks[10]. Although the present data are extremely encouraging, especially for improving basic neuroscience research, it is difficult at this stage to predict outcomes of clinical relevance, typically demonstrated through long-term chronic testing in primates. Present efforts are focused on improving low-profile headcap connector designs and developing more mechanically stable mounting media to evaluate long-term viability. Another focus is to substitute the carbon-fibre core with carbon nanotube composite materials that are stronger and more flexible than platinum in addition to being compatible with traditional microfabrication processes to enable manufacturing of high-density arrays[45]. These composite materials may negate the need for an organic recording site to detect biopotentials, and instead allow us to use these coatings for delivering bioactive molecules to the recording site[46–48]. These devices will be implanted into the brain by leveraging existing and emerging insertion techniques[49,50]. In the future, more advanced bio/nanomaterials could be used to further attenuate the tissue response and provide a more biomimetic, bio-integrating interface to further blur the line between organic and inorganic, perhaps with combinations of lipids, growth factors, cell adhesion molecules, drugs and/or enzymes[26,51]. The techniques and knowledge gained here will serve as a foundation for innovative long-term chronic implant designs that we anticipate will be transitioned to primate studies as the next step of this work.

The capability of monitoring specific neuronal ensembles for long periods of time with great precision would be a powerful tool in neuroscience research for linking low-level neuronal circuits to high-level brain function, such as learning, memory and perception. As a result of its small size, the MTE is also attractive for use with emerging optical technologies, such as *in vivo* multi-photon microscopy because it produces negligible optical shadows. These microelectrodes can also be grafted with fluorescent labels for *in vivo* multi-photon deep tissue microscopy neuroscience studies. The MTE's subcellular footprint also limits the impact of diffusion on biochemical and bioelectrical signalling around the device. Developing smaller and more flexible neural probes with advanced surface materials for long-term, high-quality and selective neural recording could potentially lead to paradigm shifts in both neuroscience research and clinical neurotechnologies. The organic integrated (nano)composite microelectrode technology may be further tailored to other disciplines, such as cardiology, peripheral nerve injury or transdermal microelectrodes, to establish stealthy bio-interfaces for monitoring and controlling intrinsic biological pathways.

Methods

Carbon-fibre MTEs

One to three individual 7-μm-diameter (Cytec Thornel T650, tensile modulus = 234 GPa) carbon fibres were mounted onto a NeuroNexus A16 printed circuit board or a bare stainless-steel wire using silver epoxy (WPI) and baked at 140 °C for 10 min. An ~800-nm-

thick poly(*p*-xylylene) insulator layer was then deposited using CVD. One gram of paracyclophane was sublimed at 90–110 °C and 0.3 mbar and carried into the pyrolysis chamber by argon at a flow rate of 20 standard cubic centimetres per minute (sccm). After pyrolysis at 670 °C, the polymer was deposited on the substrate at 15 °C. The deposition rate, according to the quartz-crystal microbalance, was 0.6–1.0 Å s^{-1}. Next, the surface was functionalized with a ~50-nm-thick poly((*p*-xylylene-4-methyl-2-bromoisobutyrate)-*co*-(*p*-xylylene)) layer using CVD. [2.2]paracyclophane-4-methyl 2-bromoisobutyrate was sublimed at 90–110 °C and 0.3 mbar and carried into the pyrolysis chamber by argon at a flow rate of 20 sccm. After pyrolysis at 550 °C, the polymer was deposited on the substrate at 15 °C at 0.6–1.0 Å s^{-1}.

ATRP

PEGMA was grafted onto the poly(*p*-xylylene) surface by ATRP. Poly((*p*-xylylene-4-methyl-2-bromoisobutyrate)-*co*-(*p*-xylylene)) was used as the initiator for ATRP because of its functional groups[28]. After deposition of poly((*p*-xylylene-4-methyl-2-bromoisobutyrate)-*co*-(*p*-xylylene)), MTEs were incubated under inert conditions with a degassed aqueous solution of oligo(ethylene glycol) methyl ether methacrylate, with CuBr/$CuBr_2$/2,2′-bipyridine as the catalyst. The polymerizations proceeded at room temperature for 4 h. Surface-modified MTEs were thoroughly rinsed after the reaction.

Recording site

Poly(*p*-xylylene)-coated and PEGMA-grafted carbon fibres were cut to a length of 0.3–0.5 cm. For PEDOT deposition, monomer 3,4-ethylenedioxythiophene (EDOT; Bayer) was electrochemically polymerized and deposited onto the surface of the electrode sites together with the anions in the solution. Specifically, PEDOT:PSS was electropolymerized from a 0.1 M PSS (Acros Organics) aqueous solution with an EDOT concentration of 0.01 M under galvanostatic conditions. In galvanostatic mode, the current was held at 100 pA.

Characterization

See Supplementary Methods for details on characterization methods: Raman spectroscopy, energy-dispersive X-ray analysis, scanning electron microscopy (SEM) imaging, EIS, cyclic voltammetry, protein adsorption and determining the stiffness and insertion force.

Surgery

The microthread probes were manually inserted into the motor cortex of adult male Sprague-Dawley rats using previously established methods[10]. The animal was anaesthetized with a mixture of 50 mg ml^{-1} ketamine and 5 mg ml^{-1} xylazine administered intraperitoneally with an initial dosage of 0.125 ml per 100 g of body weight and regular updates of ketamine. Following a craniotomy and a durotomy, a stereotaxic-frame-mounted micromanipulator guided insertions of the MTE 2 mm into the cortex. Owing to the stiffness of the carbon fibre, a 2.5–5-mm-long fibre did not need further assistance penetrating the cortex when aligned perpendicularly to the cortical surface. Surgical closure was achieved with a combination of silicone (World Precision Instruments) and Cerebond adhesive (MyNeurolab). For histology, a 5 mm Michigan silicon electrode (NeuroNexus Technologies) was inserted 500 μm away from the MTE and at least 49 μm away from all surface vessels[35]. Both probes were tethered to the skull using silicone and Cerebond adhesives. All procedures complied with the United States Department of Agriculture guidelines for the care and use of laboratory animals and were approved by the University of Michigan Committee on Use and Care of Animals. See Supplementary Methods for further details.

In vivo neural recordings

For all animals in this study, electrophysiological data were acquired using a TDT RX5 Pentusa recording system (Tucker-Davis Technologies). Neural recording segments were analysed offline, as described elsewhere[7]. Briefly, principal component analysis (PCA) was completed on isolated waveforms, and sorted using fuzzy c-means clustering. Units with sufficiently clustered principal components were plotted, and the SNR was calculated as the peak-to-peak amplitude of the mean waveform of the cluster divided by two times the s.d. of the remaining data stream after all waveforms had been removed. If a single unit was not detected, the SNR and amplitude were considered 0 and 0 μV, unless otherwise specifically stated. Recordings from the control group of chronically implanted silicon electrodes from a previous study[8] were reanalysed using these parameters. See Supplementary Methods for further details.

Vasculature and BBB disruption: acute histological imaging

Evans blue (2%) at 2 ml kg^{-1} was injected intravenously following probe insertion and then immediately perfused with 4% paraformaldehyde. See Supplementary Methods for further details.

Chronic immunohistochemistry

Rats were perfusion-fixed with 4% paraformaldehyde two weeks after implantation. Brains were dissected with devices in place. Tissue slices were cut in a direction perpendicular to the long axis of the inserted device. Sections were labelled with EBA (BBB), GFAP (astrocytes), Iba-1 (microglia), NeuN (neuron-specific nuclear protein; neuronal nuclei), laminin (BBB) and/or Hoechst. See Supplementary Methods for further details.

Supplementary Material

Refer to Web version on PubMed Central for supplementary material.

Acknowledgments

This work was financially supported by a National Institutes of Health Challenge Grant in Health and Science Research from the National Institute of Neurological Disorders and Stroke (1RC1NS068396-0110) and the Center for Neural Communication Technology, a P41 Resource Center funded by the National Institute of Biomedical Imaging and Bioengineering (P41 EB002030). A. Agarwal and F. S. Midani assisted in chronic probe assembly/packaging, chronic surgery and chronic electrophysiological recordings. A. L. Ryan and S. Saha conducted ATRP. H-Y. Chen carried out Raman spectroscopy. Multiphoton imaging of chronically implanted tissue was conducted by Wadsworth Center Advanced Light Microscopy & Image Analysis Core. L. Hains cut the tissue and conducted preliminary immunohistochemistry. Confocal images were collected on the Zeiss LSM510 at the University of Michigan Microscopy and Image Analysis Laboratory. N.A.K. and D.R.K. acknowledge partial financial support of this work from a DARPA STTR grant (W31P4Q-08-C-0426).

References

1. Strumwasser F. Long-term recording’ from single neurons in brain of unrestrained mammals. Science. 1958; 127:469–470. [PubMed: 13529005]
2. Kipke DR, et al. Advanced neurotechnologies for chronic neural interfaces: New horizons and clinical opportunities. J. Neurosci. 2008; 28:11830–11838. [PubMed: 19005048]
3. Schmidt EM, Bak MJ, McIntosh JS. Long-term chronic recording from cortical neurons. Exp. Neurol. 1976; 52:496–506. [PubMed: 821770]
4. Grill WM, Norman SE, Bellamkonda RV. Implanted neural interfaces: Biochallenges and engineered solutions. Annu. Rev. Biomed. Eng. 2009; 11:1–24. [PubMed: 19400710]

5. Biran R, Martin DC, Tresco PA. Neuronal cell loss accompanies the brain tissue response to chronically implanted silicon microelectrode arrays. Exp. Neurol. 2005; 195:115–126. [PubMed: 16045910]
6. Rousche PJ, Normann RA. Chronic recording capability of the Utah intracortical electrode array in cat sensory cortex. J. Neurosci. Methods. 1998; 82:1–15. [PubMed: 10223510]
7. Ward MP, Rajdev P, Ellison C, Irazoqui PP. Toward a comparison of microelectrodes for acute and chronic recordings. Brain Res. 2009; 1282:183–200. [PubMed: 19486899]
8. Purcell EK, Thompson DE, Ludwig KA, Kipke DR. Flavopiridol reduces the impedance of neural prostheses *in vivo* without affecting recording quality. J. Neurosci. Methods. 2009; 183:149–157. [PubMed: 19560490]
9. Kozai TDY, Vazquez AL, Weaver CL, Kim SG, Cui XT. *In vivo* two photon microscopy reveals immediate microglial reaction to implantation of microelectrode through extension of processes. J. Neural Eng. 2012; 9:066001. [PubMed: 23075490]
10. Ludwig KA, Uram JD, Yang J, Martin DC, Kipke DR. Chronic neural recordings using silicon microelectrode arrays electrochemically deposited with a poly(3,4-ethylenedioxythiophene) (PEDOT) film. J. Neural Eng. 2006; 3:59–70. [PubMed: 16510943]
11. Szarowski DH, et al. Brain responses to micro-machined silicon devices. Brain Res. 2003; 983:23–35. [PubMed: 12914963]
12. Polikov VS, Tresco PA, Reichert WM. Response of brain tissue to chronically implanted neural electrodes. J. Neurosci. Methods. 2005; 148:1–18. [PubMed: 16198003]
13. Clark JJ, et al. Chronic microsensors for longitudinal, subsecond dopamine detection in behaving animals. Nature Methods. 2010; 7:126–129. [PubMed: 20037591]
14. Van Horne CG, Bement S, Hoffer BJ, Gerhardt GA. Multichannel semiconductor-based electrodes for *in vivo* electrochemical and electrophysiological studies in rat CNS. Neurosci. Lett. 1990; 120:249–252. [PubMed: 2293112]
15. Matsumura M, Chen D, Sawaguchi T, Kubota K, Fetz EE. Synaptic interactions between primate precentral cortex neurons revealed by spike-triggered averaging of intracellular membrane potentials *in vivo*. J. Neurosci. 1996; 16:7757–7767. [PubMed: 8922431]
16. Neary JT, Kang Y, Willoughby KA, Ellis EF. Activation of extracellular signal-regulated kinase by stretch-induced injury in astrocytes involves extracellular ATP and P2 purinergic receptors. J. Neurosci. 2003; 23:2348–2356. [PubMed: 12657694]
17. Subbaroyan J, Martin DC, Kipke DR. A finite-element model of the mechanical effects of implantable microelectrodes in the cerebral cortex. J. Neural Eng. 2005; 2:103–113. [PubMed: 16317234]
18. Lee H, Bellamkonda RV, Sun W, Levenston ME. Biomechanical analysis of silicon microelectrode-induced strain in the brain. J. Neural Eng. 2005; 2:81–89. [PubMed: 16317231]
19. LaPlaca MC, Cullen DK, McLoughlin JJ, Cargill RS. 2nd High rate shear strain of three-dimensional neural cell cultures: A new *in vitro* traumatic brain injury model. J. Biomech. 2005; 38:1093–1105. [PubMed: 15797591]
20. Gilletti A, Muthuswamy J. Brain micromotion around implants in the rodent somatosensory cortex. J. Neural Eng. 2006; 3:189–195. [PubMed: 16921202]
21. Kim DH, et al. Dissolvable films of silk fibroin for ultrathin conformal bio-integrated electronics. Nature Mater. 2010; 9:511–517. [PubMed: 20400953]
22. Takeuchi S, Ziegler D, Yoshida Y, Mabuchi K, Suzuki T. Parylene flexible neural probes integrated with microfluidic channels. Lab Chip. 2005; 5:519–523. [PubMed: 15856088]
23. Rousche PJ, et al. Flexible polyimide-based intracortical electrode arrays with bioactive capability. IEEE Trans. Biomed. Eng. 2001; 48:361–371. [PubMed: 11327505]
24. Seymour JP, Kipke DR. Neural probe design for reduced tissue encapsulation in CNS. Biomaterials. 2007; 28:3594–3607. [PubMed: 17517431]
25. Cui XT, Zhou DD. Poly (3,4-ethylenedioxythiophene) for chronic neural stimulation. IEEE Trans. Neural Syst. Rehabil. Eng. 2007; 15:502–508. [PubMed: 18198707]
26. Azemi E, Lagenaur CF, Cui XT. The surface immobilization of the neural adhesion molecule L1 on neural probes and its effect on neuronal density and gliosis at the probe/tissue interface. Biomaterials. 2011; 32:681–692. [PubMed: 20933270]

27. Lahann J. Vapor-based polymer coatings for potential biomedical applications. Polym. Int. 2006; 55:1361–1370.
28. Jiang XW, Chen HY, Galvan G, Yoshida M, Lahann J. Vapor-based initiator coatings for atom transfer radical polymerization. Adv. Funct. Mater. 2008; 18:27–35.
29. Katira P, et al. Quantifying the performance of protein-resisting surfaces at ultra-low protein coverages using kinesin motor proteins as probes. Adv. Mater. 2007; 19:3171.
30. Jan E, et al. Layered carbon nanotube-polyelectrolyte electrodes outperform traditional neural interface materials. Nano Lett. 2009; 9:4012–4018. [PubMed: 19785391]
31. Harris JP, et al. Mechanically adaptive intracortical implants improve the proximity of neuronal cell bodies. J. Neural Eng. 2011; 8:066011. [PubMed: 22049097]
32. Bjornsson CS, et al. Effects of insertion conditions on tissue strain and vascular damage during neuroprosthetic device insertion. J. Neural Eng. 2006; 3:196–207. [PubMed: 16921203]
33. Ivens S, et al. TGF-β receptor-mediated albumin uptake into astrocytes is involved in neocortical epileptogenesis. Brain. 2007; 130:535–547. [PubMed: 17121744]
34. Nadal A, Fuentes E, Pastor J, McNaughton PA. Plasma albumin is a potent trigger of calcium signals and DNA synthesis in astrocytes. Proc. Natl Acad. Sci. USA. 1995; 92:1426–1430. [PubMed: 7877995]
35. Kozai TDY, et al. Reduction of neurovascular damage resulting from microelectrode insertion into the cerebral cortex using *in vivo* two-photon mapping. J. Neural Eng. 2010; 7:046011. [PubMed: 20644246]
36. Unterberg AW, Stover J, Kress B, Kiening KL. Edema and brain trauma. Neuroscience. 2004; 129:1021–1029. [PubMed: 15561417]
37. Barzo P, Marmarou A, Fatouros P, Hayasaki K, Corwin F. Contribution of vasogenic and cellular edema to traumatic brain swelling measured by diffusion-weighted imaging. J. Neurosurg. 1997; 87:900–907. [PubMed: 9384402]
38. Dixon CE, Clifton GL, Lighthall JW, Yaghmai AA, Hayes RL. A controlled cortical impact model of traumatic brain injury in the rat. J. Neurosci. Methods. 1991; 39:253–262. [PubMed: 1787745]
39. Nishimura N, Schaffer CB, Friedman B, Lyden PD, Kleinfeld D. Penetrating arterioles are a bottleneck in the perfusion of neocortex. Proc. Natl Acad. Sci. USA. 2007; 104:365–370. [PubMed: 17190804]
40. Najafi K, Suzuki K. Measurement of fracture stress, Young's modulus, and intrinsic stress of heavily boron-doped silicon microstructures. Thin Solid Films. 1989; 181:251–258.
41. Hosseini NH, et al. Comparative study on the insertion behavior of cerebral microprobes. Conf. Proc. IEEE Eng. Med. Biol. Soc. 2007; 2007:4711–4714. [PubMed: 18003057]
42. Seymour JP, Langhals NB, Anderson DJ, Kipke DR. Novel multi-sided, microelectrode arrays for implantable neural applications. Biom. Microdevices. 2011; 13:441–451.
43. Williams JC, Rennaker RL, Kipke DR. Long-term neural recording characteristics of wire microelectrode arrays implanted in cerebral cortex. Brain. Res. Brain Res. Protoc. 1999; 4:303–313. [PubMed: 10592339]
44. Luo X, Weaver CL, Zhou DD, Greenberg R, Cui XT. Highly stable carbon nanotube doped poly(3,4-ethylenedioxythiophene) for chronic neural stimulation. Biomaterials. 2011; 32:5551–5557. [PubMed: 21601278]
45. Shim BS, et al. Integration of conductivity transparency, and mechanical strength into highly homogeneous layer-by-layer composites of single-walled carbon nanotubes for optoelectronics. Chem. Mater. 2007; 19:5467–5474.
46. Keefer EW, Botterman BR, Romero MI, Rossi AF, Gross GW. Carbon nanotube coating improves neuronal recordings. Nature Nanotech. 2008; 3:434–439.
47. Luo X, Matranga C, Tan S, Alba N, Cui XT. Carbon nanotube nanoreservior for controlled release of anti-inflammatory dexamethasone. Biomaterials. 2011; 32:6316–6323. [PubMed: 21636128]
48. Cui X, et al. Surface modification of neural recording electrodes with conducting polymer/biomolecule blends. J. Biomed. Mater. Res. 2001; 56:261–272. [PubMed: 11340598]

49. Kozai TDY, Kipke DR. Insertion shuttle with carboxyl terminated self-assembled monolayer coatings for implanting flexible polymer neural probes in the brain. J. Neurosci. Methods. 2009; 184:199–205. [PubMed: 19666051]

50. Gilgunn, PJ., et al. An ultra-compliant, scalable neural probe with molded biodissolvable delivery vehicle.. Micro Electro Mechanical Systems (MEMS), 2012 IEEE 25th Int. Conf.; IEEE. 2012; p. 56-59.

51. Kotov NA, et al. Nanomaterials for neural interfaces. Adv. Mater. 2009; 21:1–35.

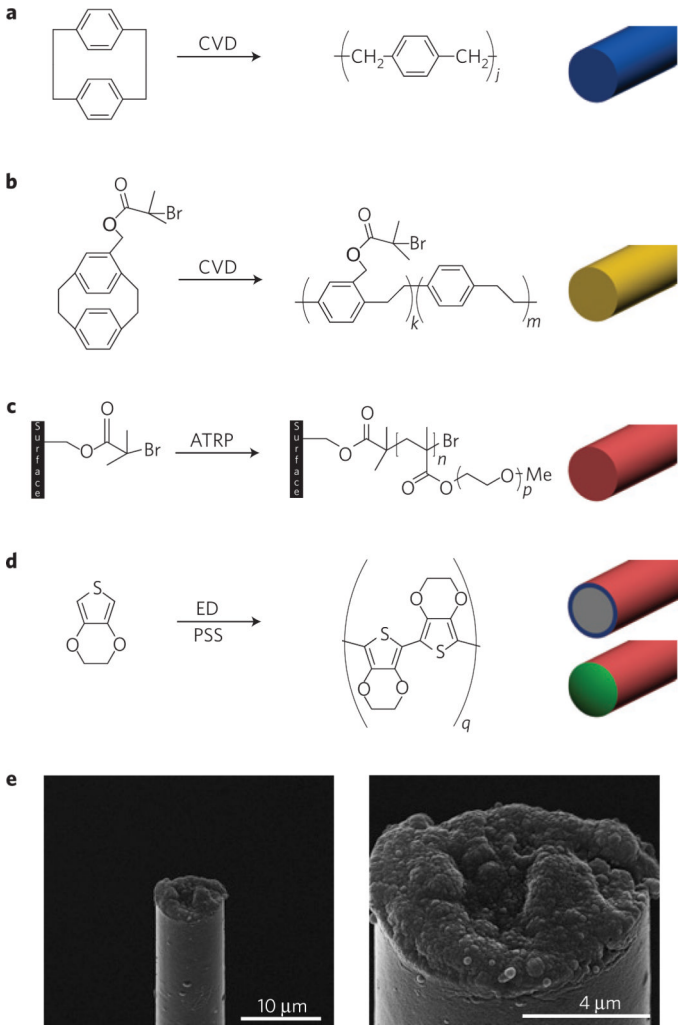

Figure 1. Microthread electrodes

a–d, Preparation of a MTE: carbon fibres are coated with 800 nm poly(*p*-xylylene) (**a**); the fibre is further coated with a 50-nm-thick layer of poly((*p*-xylylene-4-methyl-2-bromoisobutyrate)-*co*-(*p*-xylylene)) (**b**); poly(ethylene glycol) is covalently grafted onto the doubly coated fibre by ATRP (**c**); a carbon recording site is exposed at the tip by cutting away the insulation, and the recording site is coated with PEDOT by electrochemical deposition (ED; **d**). **e**, SEM images of a fully assembled, functional MTE.

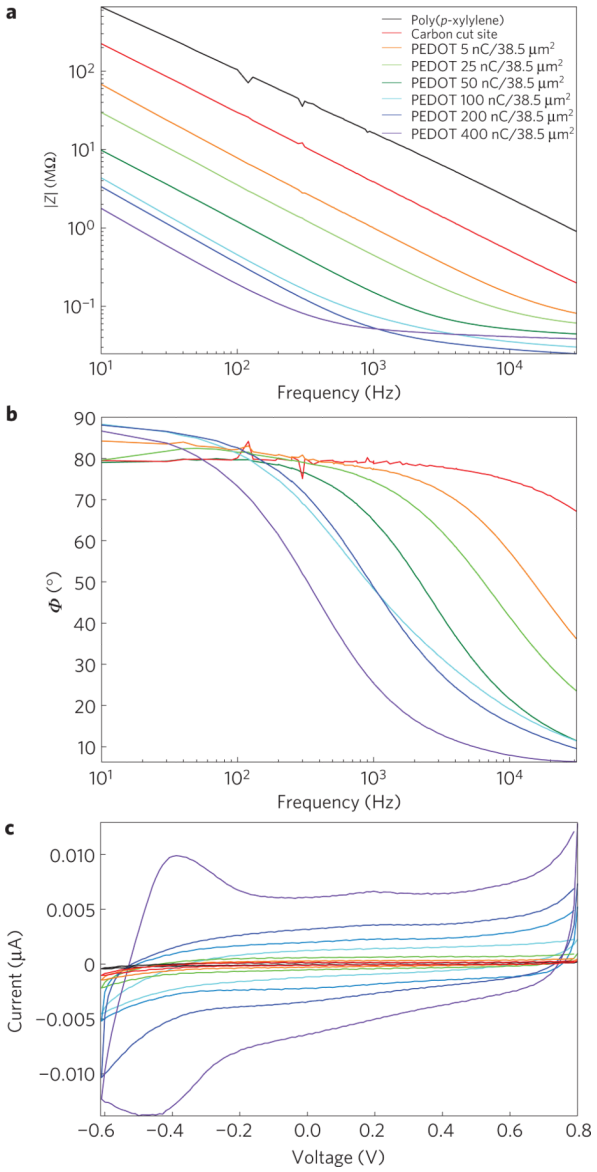

Figure 2. *In vitro* electrical characterization of MTEs

a,b, Electrical characterization of a poly(*p*-xylylene)-coated carbon fibre, a poly(*p*-xylylene)-coated fibre with an exposed carbon tip and a poly(*p*-xylylene)-coated fibre with a recording site of PEDOT:PSS electrodeposited with applied charges of 5, 25, 50, 100, 200 and 400 nC. **a**, Bode magnitude impedance plot showing decreasing impedance with increasing PEDOT deposition across all frequencies. **b**, Bode phase plot showing phase shift towards smaller phases indicative of a change from a capacitive carbon interface to a faradaic PEDOT interface with increasing deposition. The poly(*p*-xylylene)-insulated fibre without an exposed recording site was not plotted because a reliable signal could not be detected. **c**, Cyclic voltammogram showing increasing charge storage capacity with increasing PEDOT deposition in response to voltage cycling of the electrode site.

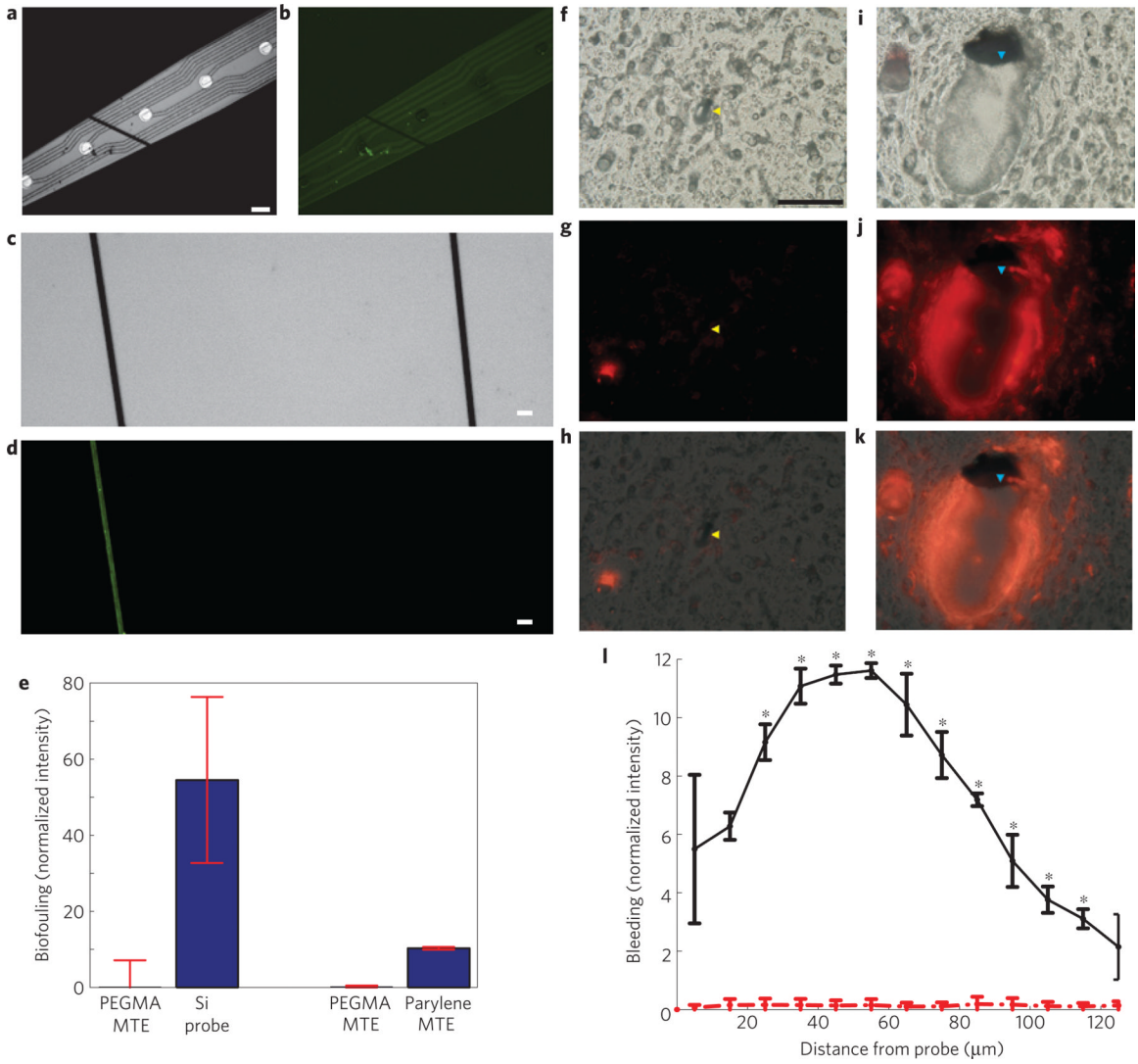

Figure 3. Physical characteristics of the MTEs

a, A MTE laid on top of a 10 mm silicon electrode. Scale bar, 50 μm. **b**, FITC–albumin adsorbed onto a 10 mm silicon electrode whereas an ATRP-PEGMA surface-coated MTE showed no adsorption. **c**, Bright-field images of FITC–albumin adsorbed onto a poly(*p*-xylylene)-coated device (left) and an ATRP-PEGMA coated device (right). Scale bar, 20 μm. **d**, The same image as in **c** under fluorescent microscopy showing less protein adsorption onto the PEGMA surface (right) compared with the poly(*p*-xylylene) surface (left). **e**, Comparison of the intensity of adsorbed FITC–albumin between PEGMA-coated MTEs and silicon probes (left), and PEGMA coated MTEs and poly(*p*-xylylene)-coated MTEs. Error bars show s.d. **f–k**, Comparison of acute BBB disruption caused by MTE probes (yellow arrowhead; **f–h**) and silicon probes (blue arrowhead; **i–k**) during insertion into the rat cortex. **f**, Differential interference contrast image of a rat motor cortex section around a MTE footprint. Scale bar, 100 μm. **g**, A BBB impermeable fluorescent dye was used to image the vasculature and bleeding around the MTE. **h**, Overlay of images in **f,g. i**, Differential interference contrast image of a 5 mm silicon probe in the same section. **j**, Bleeding around the silicon probe. **k**, Overlay of images in **i,j. l** ,Radial intensity profile indicating bleeding around silicon electrodes (solid black) and MTEs (dashed red). Error bars show s.e.m.; indicates statistical significance, $p < 0.05$.

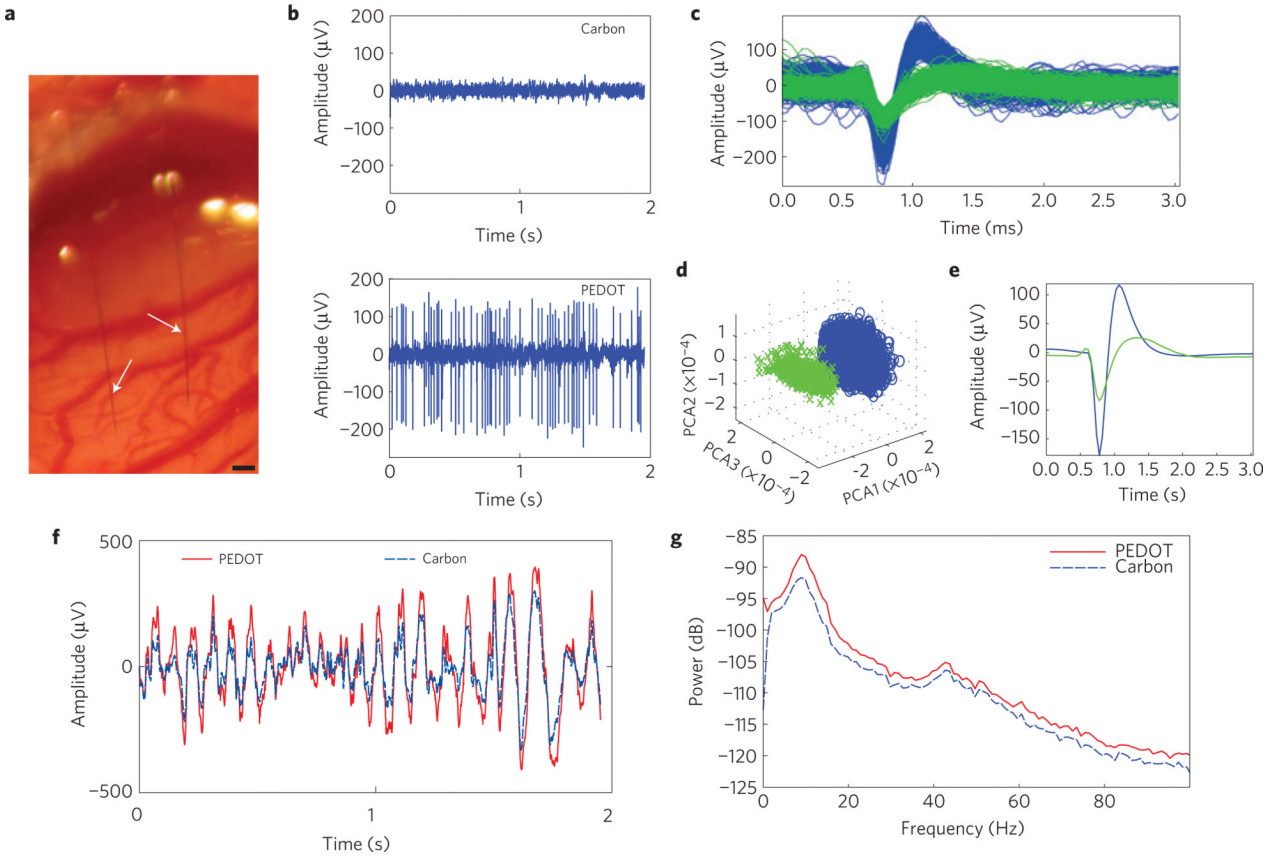

Figure 4. ***In vivo*** **single-unit recording capabilities**

a, MTA stereotrode (arrows) implanted 1.6 mm deep into the cortex. Scale bar, 100 μm. **b**, Representative example of 2 s of high-speed recordings taken simultaneously on the same array. Recordings on the carbon site channel show no discernible single units with a noise floor of 16.6 μV (top), whereas recordings taken on the channel with the PEDOT:PSS site show SNRs of 12.7 and 4.71 and a noise floor of 23.4 μV (bottom). **c**, Piled single-unit neural recordings over 3 min from a poly(*p*-xylylene)-coated PEDOT:PSS device. **d**, Results from PCA showing two distinct clusters. **e**, Mean waveform for each unit spike. **f**, Raw LFP simultaneously recorded across both channels. The PEDOT:PSS site channel recorded a noise floor of 332 μV (solid red), whereas the carbon site channel recorded a noise floor of 233 μV (dashed blue). **g**, Power density spectra across the LFP range showing that for the LFP range both recording materials are similar.

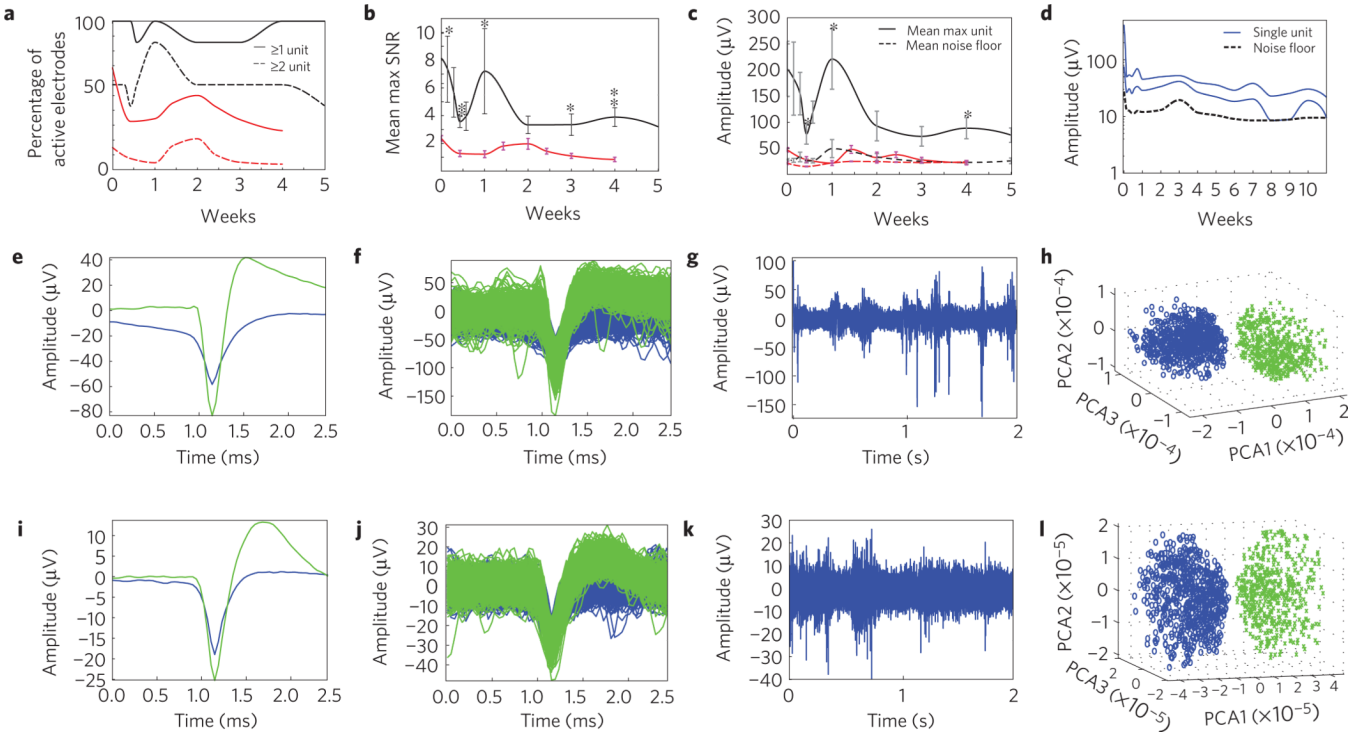

Figure 5. Chronic *in vivo* recording capabilities of MTEs

a, Percentage of active chronically implanted MTEs (black, $N = 7$) and silicon probes (red, $N = 80$ sites, 5 probes) able to detect at least 1 single unit (solid line) or at least 2 single units (dashed line) as a function of weeks post-implantation. **b**, Mean SNR of the largest single unit detected on each electrode for MTE (black, $N = 7$) and silicon probes (red, $N = 80$). Error bars indicate s.e.m.;* and ** indicate two-tailed, unequal variance statistical significance, $p < 0.05$ and $p < 0.01$, respectively. **c**, Mean amplitude of the largest single unit detected on each electrode (solid line), and the mean noise floor of each electrode (dashed line) for MTEs (black, $N = 7$) and silicon electrodes (red, $N = 80$). Error bars indicate s.e.m.; * indicates two-tailed, unequal variance statistical significance, $p < 0.05$. **d**, Amplitude of two distinct single units detected on the same electrode from the longest implant (solid, blue) starting at 408 μV on day 0. Amplitude of the noise floor from the same animal (dashed, black). For the purpose of this figure, when only one single unit was detected, the second amplitude was considered to be the same as the noise floor. **e–h**, Electrophysiological recordings taken from a rat with a MTE implanted in M1 five weeks post-implantation. **i–l**, Electrophysiological recordings taken from a different rat implanted with a MTE in M1 seven weeks post-implantation. **e,i**, Mean waveform of discernible single units. **f,j**, Piled single units from 2 min of recordings. **g,k**, Representative example of 2 s of high-speed recordings. **h,l**, Results from PCA showing distinct clusters.

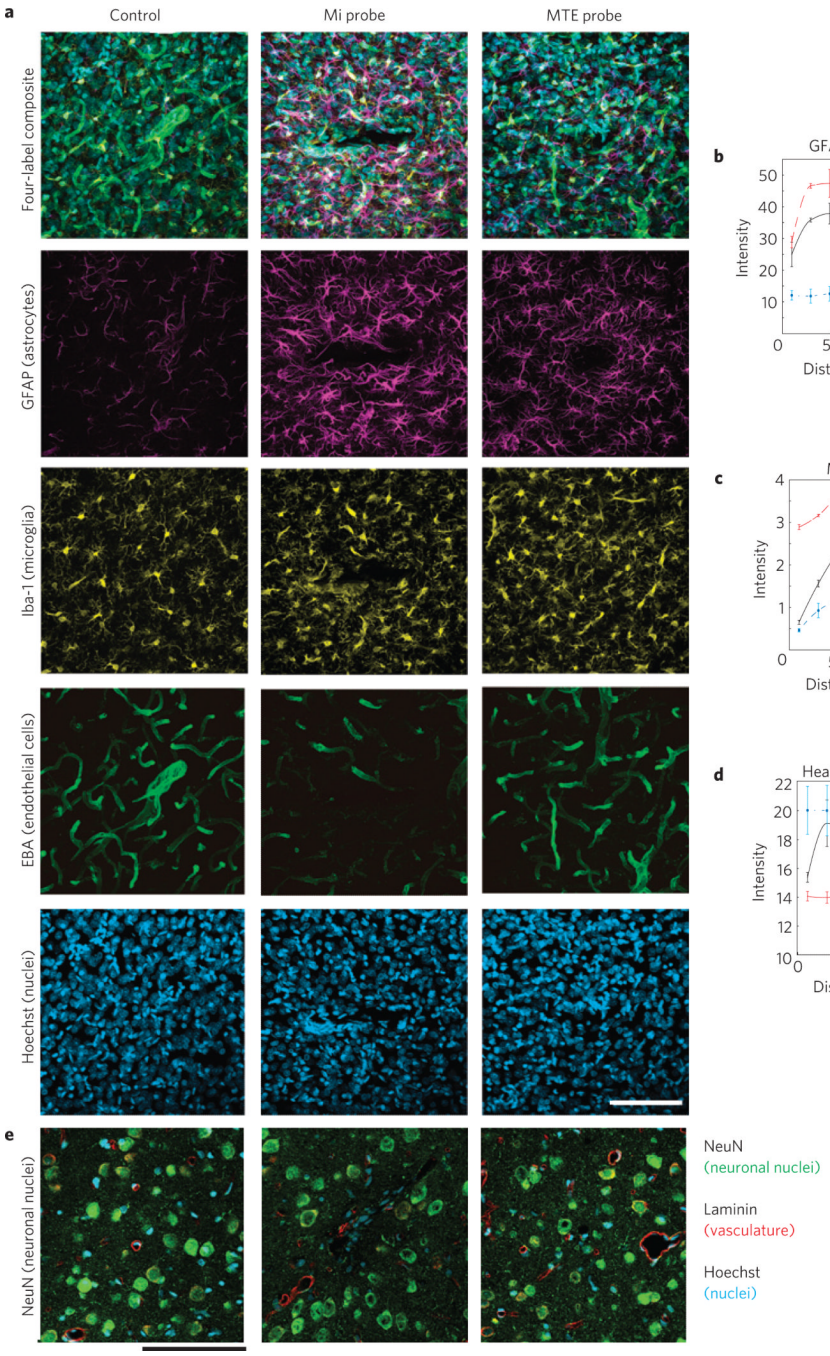

Figure 6. Histological comparison of tissue reaction to chronically implanted microthread and silicon probes

a, Tissue responses in motor cortex following a two-week implantation of a planar silicon electrode (centre), MTE (right) and a negative control from the contralateral hemisphere (left). Tissues are labelled for astrocytes (purple), microglia (yellow), BBB/endothelial cells (green) and nuclei (blue). Scale bar, 100 μm. **b–d**, Fluorescent intensity profile with increasing distance from the probe surface for MTE (solid black), silicon probe (dashed red) and control tissue (dash–dot blue). Error bars show s.e.m. **b**, Astrocyte GFAP activity. **c**, Microglia IBA-1 intensity. **d**, Healthy endothelial cells. **e**, Neurons (green), vasclature (red) and cell nuclei (blue) of a planar silicon electrode (centre), MTE (right) and a negative

control from the contralateral hemisphere (left) from a separate tissue sample. Scale bar, 100 μm.

Table 1

Mechanical properties of silicon electrodes versus MTEs.

	Cross-sectional area (μm^2)	Flexibility, compliance (axial; m N^{-1})	Flexibility, compliance (planar; m N^{-1})	Flexibility, compliance (lateral; mN^{-1})	Fracture strength (MPa)	Insertion force (mN)	Biofouling (normalized intensity)
Si probe	3,000	4.04×10^{-6}	0.289	0.00163	1,800	40	54.5 ± 21.8
MTE probe	58.1	2.20×10^{-4}	94.3	94.3	4,550	1.26×10^{-15}	0.214 ± 6.99